# A Simple Model for the Propagation of Internally Reflected Light through a Scintillator and Light Guide System

W. Brooks
October 1994

## 1. Introduction

This document describes a project undertaken as a part of the Summer Institute for Teacher Enhancement (SITE) program at CEBAF in the summer of 1993. This is a program funded by the U. S. Department of Energy Office of Science Education and Technical Information. The focus of this program is to help teachers become partners in the scientific community by participating in research projects at national research facilities under the mentorship of scientific staff. Teams of several precollege level science teachers work in collaboration on a project which is relevant to the scientific program at the institution and thereby the teachers become collaborators in the research. These assignments are intended to be true research projects which can be accomplished within the time frame of the program. As in any real research endeavor, the time required to finish the project is not completely predictable and accomplishing the goal requires much learning of new ideas and methods, trying different approaches with both successes and failures, changing strategies mid-stream, and working together as a group.

The project described herein involved significant contributions by a number of people. The group of teachers were mentored by Will Brooks (CEBAF); the teachers were:

Elma Brown
Greensville County High School, Emporia, VA

Maria Cooper
Tallwood High School, Virgina Beach, VA

Randolf Reed
Hayes Junior High School, St. Albans, WV

Rickey Ross
Blair Middle School, Virgina Beach, VA

Harriet Williams
Smithfield Elemetary School, Windsor, VA

In addition to those listed above, thanks go to a number of others: Stan Majewski, Carl Zorn, Randy Wojick and Drew Weisenberger of the CEBAF Detector Meisters gave

guest lectures and demonstrations; Volker Burkert (CEBAF) suggested the project topic and provided input to its progress; Willie Cooper (spouse of one of the teachers) wrote a program to scan hardcopies of plots and digitize their values; and Stepan Stepanyan, Gegam Asryan and Raphael Demirchyan (Yerevan Physics Institute) provided a great deal of help in performing the experimental measurements which constrained the model calculation.

This project is an example of the kind of far-reaching influence which basic research institutions can have on a society. First, the teachers involved became more knowledgeable and enthusiastic about science, and in turn in the following year shared their enthusiasm and insights with their students. As a result these students will be better qualified and more interested in science and technology as a career goal, and will grow up to be more scientifically literate citizens. In a second direction, the quantitative results of the study have motivated CEBAF staff to suggest to the major domestic manufacturer of scintillator material to modify one of their product lines to be more optimal for optical systems of the type described below. This manufacturer has responded by offering a new product which has in turn been tested at CEBAF with promising results. Since scintillator and fiber products are increasingly used in a variety of applications including many medical subfields, this chain of events has already had a small but positive and broad-based influence on industry. In times of shrinking support and appreciation for basic research it is important and instructive to note these kinds of fundamental connections between basic science, education, and industry.

## 2. Definition of the Project

The original title of the project was "Developing a Model for the Spectral and Temporal Evolution of Light Pulses through the CEBAF Large Acceptance Spectrometer (CLAS) Electromagnetic Shower Calorimeter". The Electromagnetic Shower Calorimeter (ESC) is a large particle detector which consists of alternating layers of 1 cm thick plastic scintillator material and 2.3 mm thick lead sheets for a total of 39 layers of each. The layers of scintillator are comprised of strips of plastic approximately 10 cm wide varying in length from 20 cm to over 400 cm. The primary function of any scintillator is to convert energy lost by subatomic particles passing through its volume into light which is then sampled by a light propagation and measurement system. In this system the light from the scintillators is transported first through the scintillator, then through an array of 3 mm diameter cladded plastic optical fibers, then through a conventional mixing light guide; at this point it reaches the photomultiplier tube. In a system such as the ESC the optical elements in the system

each have absorption characteristics which significantly modify the initial emission spectrum of the scintillator's fluors. Thus it is interesting and useful to consider the details of the process of light propagation through the system.

The goal of this project was to take the measured absorption characteristics of each of the optical elements in the ESC together with the indices of refraction and measured light emission curve of the scintillator and predict 1) the resulting light spectrum, 2) the time dispersion associated with path length variations, and 3) the variation of light intensity of the system as a function of light source position along the scintillator.

## 3. Definition of the Model and Calculation Method

A standard method for developing a model of a light transport system is to use a Monte Carlo ray-tracing program. Such a program would generate rays with a distribution of wavelengths and over a range of solid angles and would then follow the development of the intensity of each ray through each geometry and material type in the system. (Ray optics is considered to be sufficient for this purpose.) In this project this approach was not taken because none of the teachers had proficiency in scientific programming; however each had experience with personal computers and with the use of spreadsheets. It was decided to attempt to develop this model within a *spreadsheet* computing environment and to adapt the level of complexity of the model to this requirement.

Given this constraint, the model is the following. A light emission profile for the scintillator as a function of wavelength is the starting point for the computation. For each wavelength, the path lengths of rays are computed as a function of angle assuming light is emitted at the *center of a cylindrical light guide*. This is expected to reproduce many properties of the system since in the absence of reflection losses the evolution of the system can be described in terms of general concepts such as phase space incompressibility[1], completely independent of the light guide geometry. The assumption of a point source is expected to limit the accuracy of reproducing the measured data close to the readout end of the scintillator, since in the data the light source is distributed over a volume.

The number of rays calculated in a given angle range is *proportional to solid angle*. The angle of the light rays referred to throughout this document is the polar angle with respect to the z axis defined by the cylindrical axis of symmetry. (Note that this is not the normal angle to the surface of reflection, but rather its complement in cylindrical symmetry.) From the angle-dependent path length of each ray at a given wavelength a purely *exponential attenuation* is calculated; the average of the intensities gives a solid-angle-weighted wavelength distribution. This procedure is followed for each optical

element in the system, where the input to each successive calculation is the spectral output distribution from the previous element. This is simply a numerical integration over the wavelengths and angles in the light transport problem.

The maximum angle considered is the largest angle due to *total internal reflection,* which is given by the index of refraction. This is an important input parameter in this model. Note that the model does not consider light which is not totally internally reflected.

In addition to light attenuation by self-absorption, an attempt has been made to include *reflection losses* for each ray, an effect which does in fact depend on the lightguide geometry. This is accomplished assuming a formula derived for a point light source in the center of a cylindrical light guide for the number of reflections as a function of distance for a given angle, slightly modified for a rectangular geometry. This is expected to be a good assumption for a sufficiently long light guide. Thus the reflection loss calculation is not expected to perform well for short scintillator lengths, but should improve for longer scintillators. The formulas used in the reflection loss parameterization are the following:

$$\text{Final intensity } (\theta) = (1.0 - \gamma)^N \text{ initial intensity } (\theta)$$

$$\text{Number of reflections} = N = \text{INT}[x\tan(\theta)/(D - \alpha\sin(\theta)) + 0.5]$$

In these equations x is the length of the scintillator through which light travels, $\theta$ is the polar angle defined previously, and $\alpha$, $\gamma$ and D are explained below. There are only *two free parameters* in the reflection loss calculation - the average light loss per reflection $\gamma$, and a second geometrical parameter $\alpha$ written in the equation above. This second parameter expresses the deviation of the reflection probability in a rectangular system from that of a cylindrical system; when its value is set to zero, the formula for a cylindrical system is recovered. These two free parameters are obtained by comparing calculations to data. A third parameter in this formula is the diameter of the light guide D. Since the light guide is not actually cylindrical this value is an "effective diameter" and the parameter is fixed by simple geometrical arguments to be 1.273 cm. Reflection losses were only computed for the scintillator and not for either of the light guides.

## 4. Description of the System

A schematic diagram of the optical system of the ESC is given in Fig. 1. The light originates in a rectangular scintillator which can have the longest length dimension of any

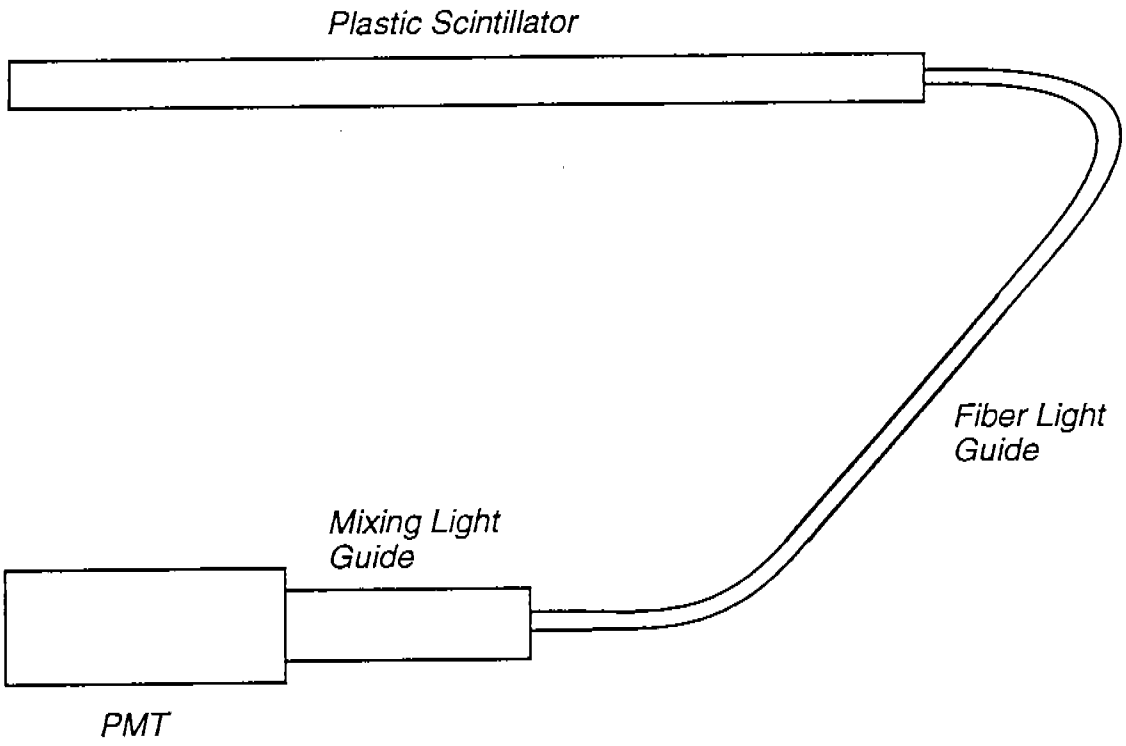


Fig. 1 A schematic drawing of the optical system. The light pulse originates in the scintillator, then travels through the fiber light guide, the mixing light guide, and finally enters the photomultiplier tube.

element in the system. The emitted light propagates from the origination point through the scintillator to the fiber light guide, being partially re-absorbed in path length- and wavelength-dependent processes. The light then passes into the fiber light guide, at which point the intensity is reduced by the ratio of the cross sectional area of the fibers to that of the scintillator (and in addition by coupling losses and an approximately 11% reflection loss due to the air gap coupling). A mixing light guide follows the fibers, and then the light is absorbed with a wavelength dependent efficiency by the photo cathode of a photomultiplier tube. Some light is absorbed in each optical element, and this absorption depends on the wavelength and average path length of the light.

## 5. Description of the Measurements

While a primary result of the calculation is the final light spectrum, this quantity is not easily measured for such a large system. The measurements performed by the teachers involved moving a radioactive source along a scintillator and measuring the light output of the system under several circumstances. The method has been described elsewhere for an X-ray source [2].

Since the rate from the source is constant, the light intensity depends on the cumulative light absorption as a function of distance along the scintillator. This can be calculated in this model and so provides a test of the validity of the model.

Four of the teachers' measurements are plotted in Fig. 2. The top curve was made by coupling the photo tube directly to the scintillator using optical coupling gel (no light guides were used; referred to as the "direct" readout method). The second curve was made under the same conditions with no coupling gel. The third curve from the top was made with the entire system described in the previous section, using a short (18 cm) fiber light guide. The fourth curve was made under the same conditions, but using a long (85 cm) fiber light guide. An adjustment to the data had to be made to be able to compare the currents of the upper two curves with the lower two, due to the very different intensities measured in the two arrangements. Therefore the absolute normalization between the two data sets is not known accurately. Because of this, no attempt is made to explain the relative intensities, even though this is in principle possible.

## 6. Inputs to the Calculation

The inputs to the calculation as mentioned above are plotted in Fig. 3 - 7; the indices of refraction used were 1.58, 1.6, 1.49, and 1.495 for the scintillator, fiber core, fiber

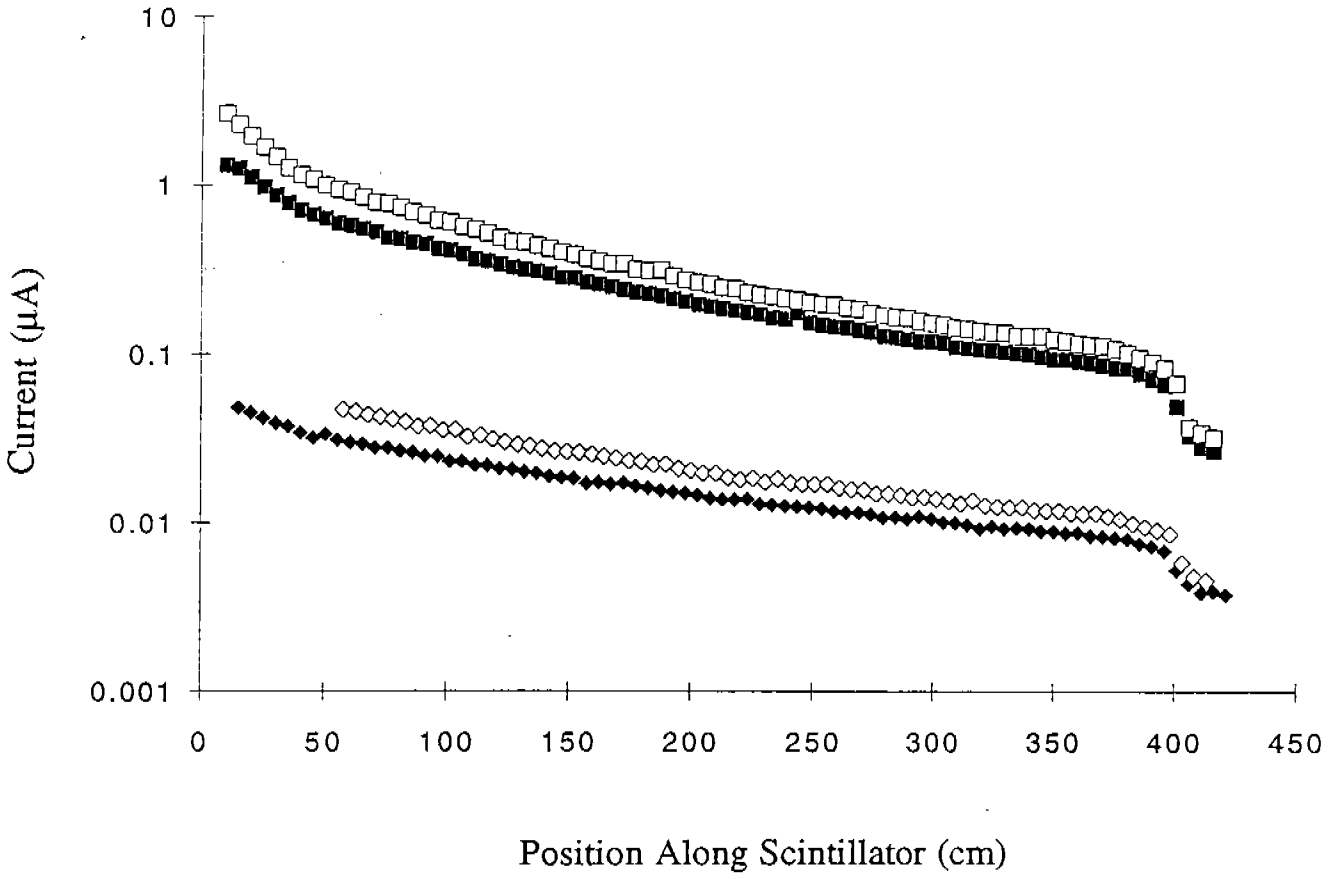


Fig. 2 Four sets of data measured by the teachers. The uppermost curve was taken with the photomultiplier tube directly coupled to the scintillator with coupling gel. The next curve was measured in the same way without coupling gel. The third curve was taken with the full 4-element system pictured in Fig. 1 with a short (18 cm) fiber light guide. The bottom curve was measured in the same way with a long (85 cm) fiber light guide.

cladding, and mixing light guide, respectively. In Fig. 3 is shown the emission spectrum of BC-412 scintillator made by Bicron Corp. This data has been obtained from the manufacturer [3]. Fig. 4 shows the attenuation length of BC-412 as a function of wavelength. This was derived from a fit to absorption data. The two curves indicated are for a fixed value of the reflection coefficient for the plastic and for a fitted value, and the difference between the curves may be taken as an indication of the uncertainty in the measurement. In Fig. 5 the attenuation length as a function of wavelength for the fiber light guide material, Bicron BCF-98, is shown. This data was also derived from attenuation measurements on a number of samples of 3 mm diameter fiber. Fig. 6 shows the same type of plot for the mixing light guide. The nature of the two curves is the same as for Fig. 4; here there is a greater uncertainty because the samples of the acrylic light guide came from two different sources, and therefore had different surface qualities as well as potentially different bulk properties. All the data shown in Fig. 4 - Fig. 6 are derived from absorption data taken by Carl Zorn (CEBAF). Fig. 7 shows the absorption efficiency of the photo cathode of the photomultiplier tube as supplied by the manufacturer [4]. An additional input to the calculation was a list of angles for the rays which were weighted according to solid angle. These were generated by a separate program.

The indices of refraction were used to calculate the maximum total internal reflection angles in each optical element. For the computation to compare to the measured data, the maximum angles used were 50.7°, 39.3°, and 21.6° for the cases of direct coupling with gel, direct coupling without gel, and the fiber readout system respectively. This wide variation in internal reflection angles allowed a very good determination of the two reflection loss free parameters, within the accuracy of the overall model.

## 7. Spreadsheet Layout

An example of the spreadsheet layout is given for the scintillator section alone in Fig. 8. In the spreadsheet program used it was possible to write a "subroutine" to loop through all calculations as one might do in a conventional program. However, this approach was not taken here for several reasons. For people used to conventional applications of a spreadsheet it is more familiar to have the results of all calculations displayed at all times. In addition this is also quite convenient for troubleshooting the calculation. Finally, laying out the spreadsheet in block format is a natural visualization tool to identify the key concepts in the calculation. The (input) initial intensity spectrum is given as a vertical column on the left, as are the attenuation lengths as a function of wavelength. The angles are labeled in a row along the top. Path lengths for a given angle

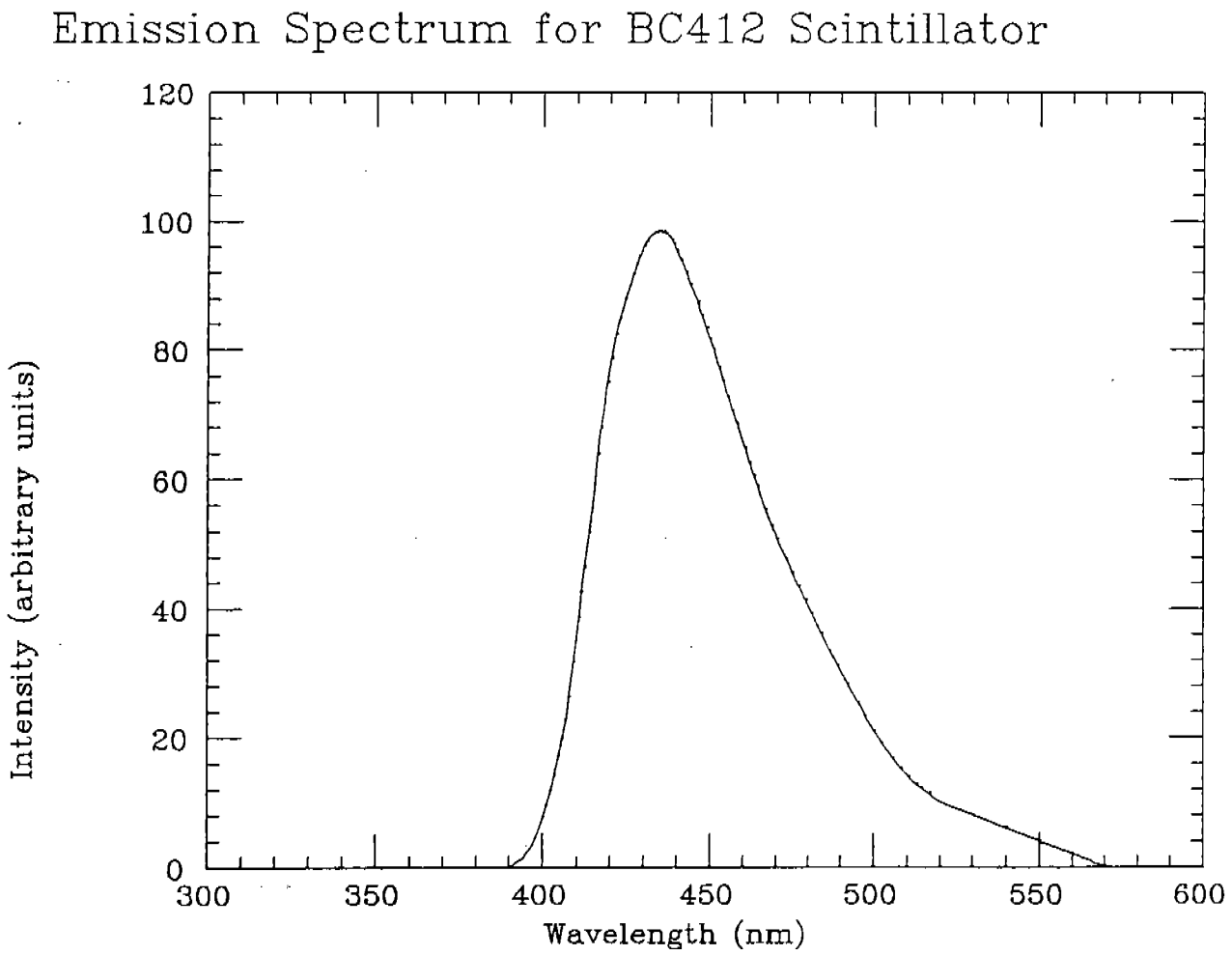


Fig. 3 Light emission spectrum for BC412 scintillator.

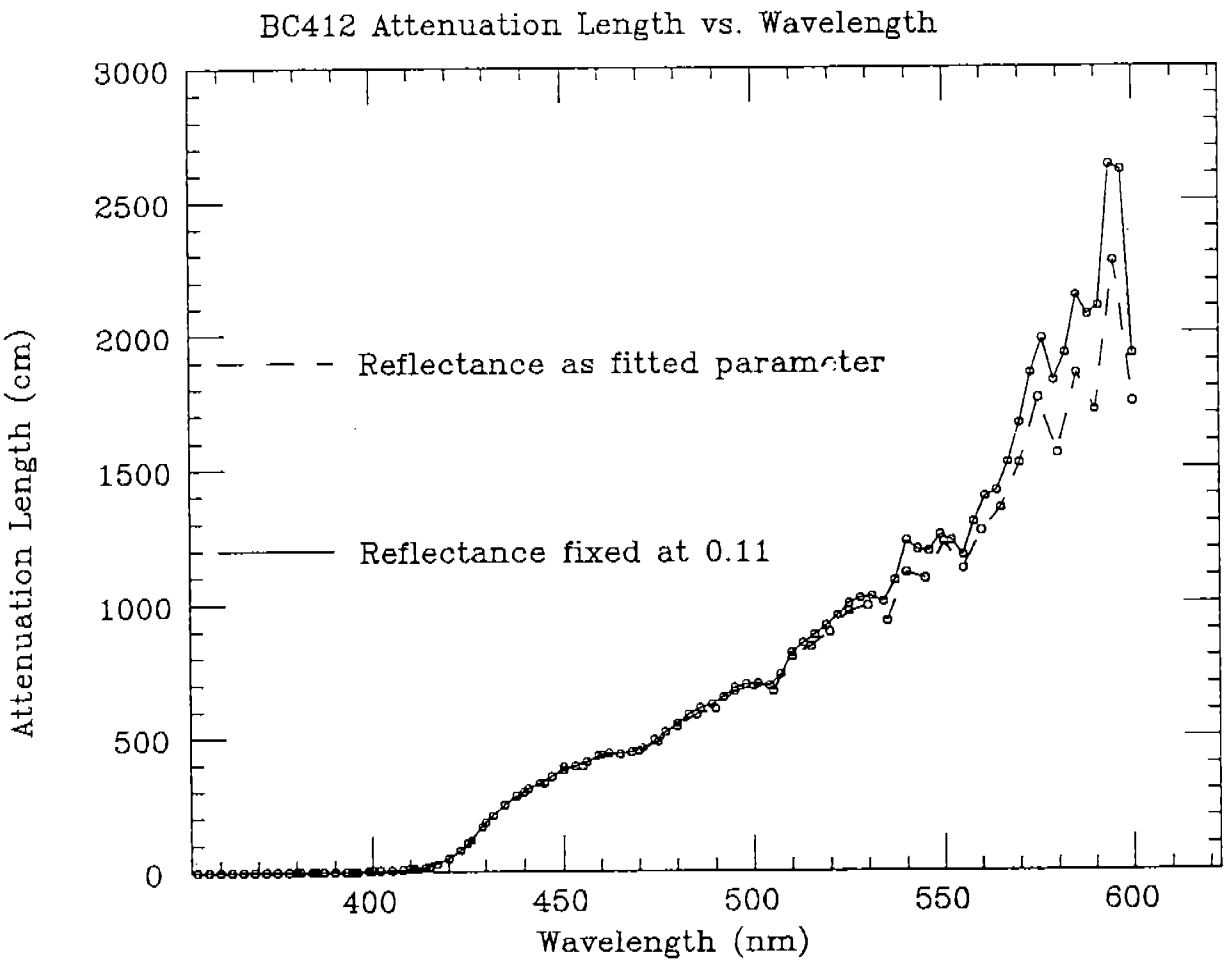


Fig. 4 Attenuation length of BC412 scintillator as a function of wavelength.

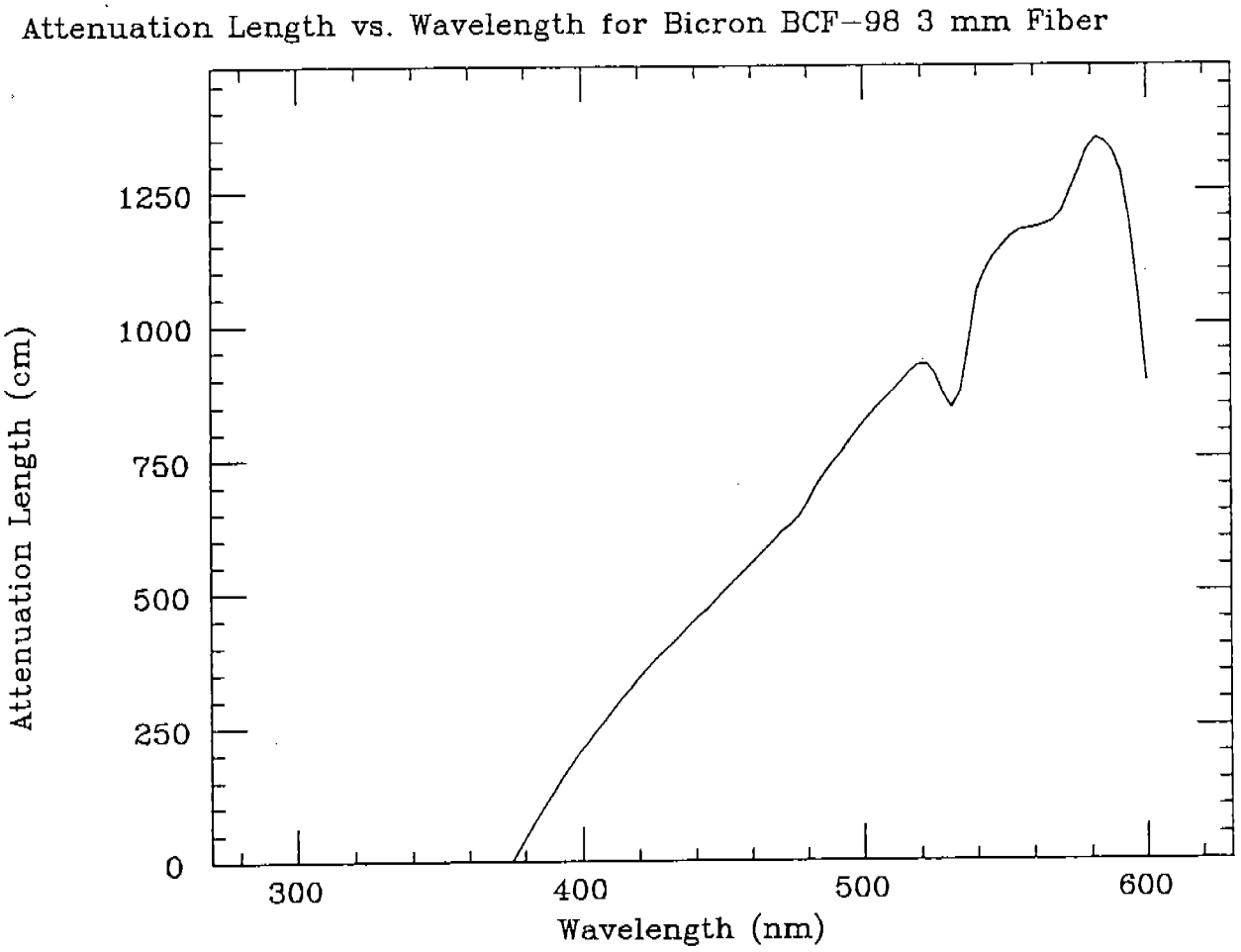


Fig. 5 Attenuation length of BCF-98 coated plastic fiber as a function of wavelength.

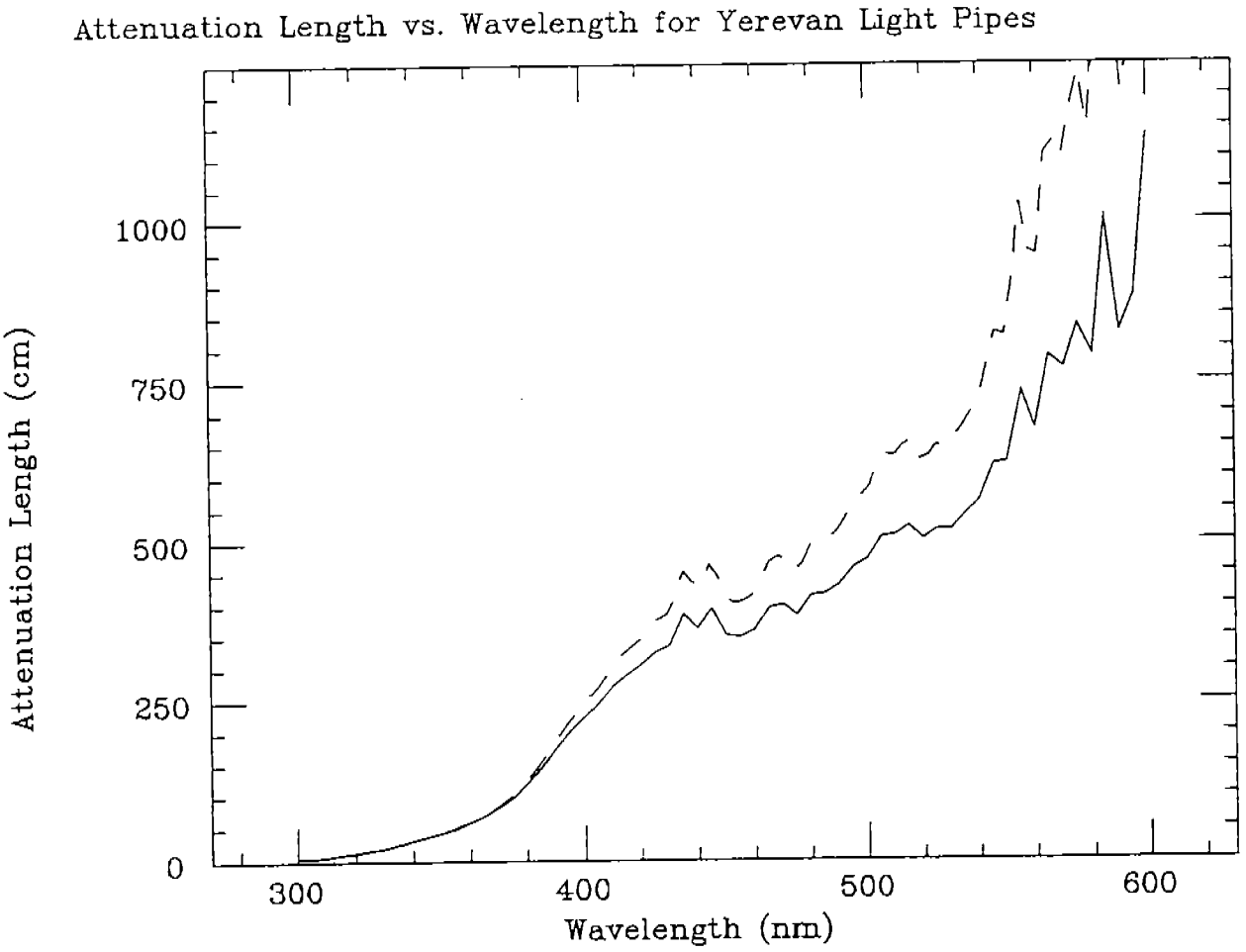


Fig. 6 Attenuation length of Yerevan-made acrylic mixing lightguide as a function of wavelength.

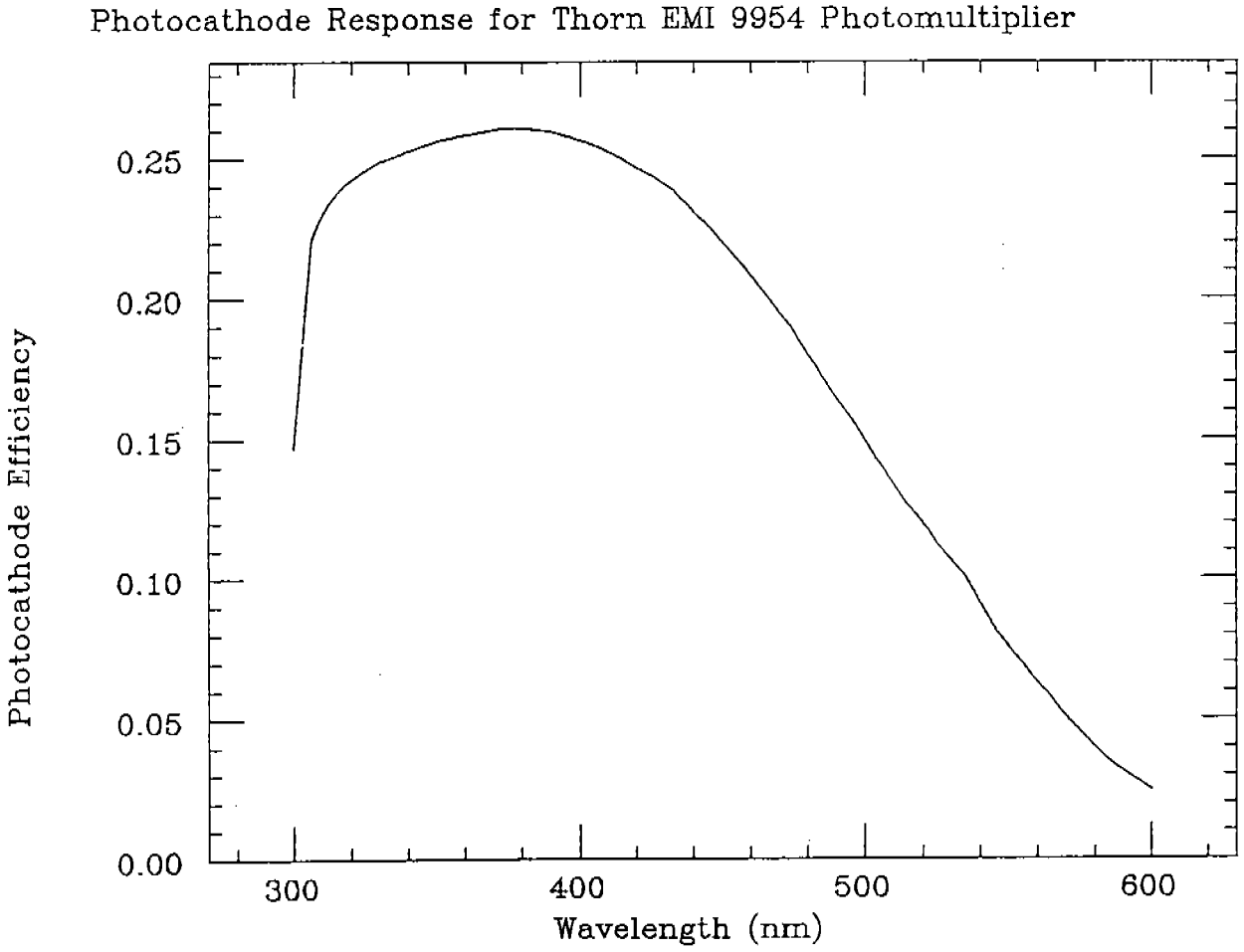


Fig. 7 Absorption efficiency of the photomuliplier photocathode as a function of wavelength.

| Wavelength (nm) | Scintillator Attenuation Length (cm) | Scintillator Emission Spectrum (attenuated) | Angles: Degrees: | 0 | 2.15227 | 3.043 | 21.54018 | 21.65 | Spectrum after Scintillator: |
|---|---|---|---|---|---|---|---|---|---|
| | | | Radians: | 0 | 0.03756 | 0.053 | 0.37595 | 0.37786 | |
| 300 | 1.92803 | 0 | | 0 | 0 | | 0 | 0 | 0 |
| 303 | 1.729734 | 0 | | 0 | 0 | | 0 | 0 | 0 |
| 306 | 1.546649 | 0 | | 0 | 0 | | 0 | 0 | 0 |
| 309 | 1.378171 | 0 | | 0 | 0 | | 0 | 0 | 0 |
| 312 | 1.223695 | 0 | | 0 | 0 | | 0 | 0 | 0 |
| 315 | 1.082616 | 0 | | 0 | 0 | | 0 | 0 | 0 |
| 318 | 0.9543288 | 0 | | 0 | 0 | | 0 | 0 | 0 |
| 321 | 0.8382293 | 0 | | 0 | 0 | | 0 | 0 | 0 |
| 324 | 0.7337124 | 0 | | 0 | 0 | | 0 | 0 | 0 |
| 327 | 0.6401733 | 0 | | 0 | 0 | | 0 | 0 | 0 |
| 330 | 0.5570071 | 0 | | 0 | 0 | | 0 | 0 | 0 |
| 333 | 0.483609 | 0 | | 0 | 0 | | 0 | 0 | 0 |
| 336 | 0.4193744 | 0 | | 0 | 0 | | 0 | 0 | 0 |
| 339 | 0.3636982 | 0 | | 0 | 0 | | 0 | 0 | 0 |
| 342 | 0.3159758 | 0 | | 0 | 0 | | 0 | 0 | 0 |
| 345 | 0.2756024 | 0 | | 0 | 0 | | 0 | 0 | 0 |
| 348 | 0.241973 | 0 | | 0 | 0 | | 0 | 0 | 0 |
| 351 | 0.2144829 | 0 | | 0 | 0 | | 0 | 0 | 0 |
| 354 | 0.1925274 | 0 | | 0 | 0 | | 0 | 0 | 0 |
| 357 | 0.1755015 | 0 | | 0 | 0 | | 0 | 0 | 0 |
| 360 | 0.1628004 | 0 | | 0 | 0 | | 0 | 0 | 0 |
| 363 | 0.1538195 | 0 | | 0 | 0 | | 0 | 0 | 0 |
| 366 | 0.1479537 | 0 | | 0 | 0 | | 0 | 0 | 0 |
| 369 | 0.1445985 | 0 | | 0 | 0 | | 0 | 0 | 0 |
| 372 | 0.1431488 | 0 | | 0 | 0 | | 0 | 0 | 0 |
| 375 | 0.143 | 0 | | 0 | 0 | | 0 | 0 | 0 |
| 378 | 0.1435472 | 0 | | 0 | 0 | | 0 | 0 | 0 |
| 381 | 0.1442702 | 0 | | 0 | 0 | | 0 | 0 | 0 |
| 384 | 0.1455448 | 0 | | 0 | 0 | | 0 | 0 | 0 |
| 387 | 0.1537469 | 0 | | 0 | 0 | | 0 | 0 | 0 |
| 390 | 0.177 | 0 | | 0 | 0 | | 0 | 0 | 0 |
| 393 | 0.1678053 | 0.11777985 | | 0 | 0 | | 0 | 0 | 0 |
| 396 | 0.5480897 | 0.34356496 | | 0 | 0 | | 0 | 0 | 0 |
| 399 | 1.151469 | 0.76819491 | 1.045E-151 | | 7.656E-152 | 5.793E-1 | 604E-163 | 1.196E-163 | 4.299E-153 |
| 402 | 1.752981 | 1.41649578 | 1.129E-99 | | 8.996E-100 | 7.406E-1 | 336E-107 | 1.097E-107 | 6.535E-101 |
| 405 | 2.363 | 2.25220716 | 6.8679E-74 | | 5.7042E-74 | 4.8959E- | 7715E-80 | 5.836E-80 | 5.0819E-75 |
| 408 | 5.191018 | 3.37047354 | 1.1551E-33 | | 1.0239E-33 | 9.3803E- | 1579E-36 | 1.0757E-36 | 1.6125E-34 |
| 411 | 9.435301 | 5.07941658 | 1.9694E-18 | | 1.789E-18 | 1.6796E | 2.565E-20 | 2.5464E-20 | 4.249E-19 |
| 414 | 15.23195 | 6.65885178 | 2.6216E-11 | | 2.4087E-11 | 2.2874E | 1913E-12 | 1.1533E-12 | 7.5377E-12 |
| 417 | 25.09108 | 8.40859866 | 1.0028E-06 | | 9.2813E-07 | 8.8785E | 8892E-08 | 9.6547E-08 | 3.6137E-07 |
| 420 | 45.528 | 9.75385026 | 0.00149125 | | 0.00138712 | 0.00133 | 00025167 | 0.00024714 | 0.00064341 |
| | | | | | | | | | |
| 567 | 1520.655 | 0.0756 | 0.0581143 | | 0.05438258 | 0.0 | 0.01859847 | 0.01839052 | 0.03197191 |
| 570 | 1665.811 | 0 | 0 | | 0 | | 0 | 0 | 0 |
| 573 | 1852.151 | 0 | 0 | | 0 | | 0 | 0 | 0 |
| 576 | 1981.549 | 0 | 0 | | 0 | | 0 | 0 | 0 |
| 579 | 1824.699 | 0 | 0 | | 0 | | 0 | 0 | 0 |
| 582 | 1925.703 | 0 | 0 | | 0 | | 0 | 0 | 0 |
| 585 | 2142.449 | 0 | 0 | | 0 | | 0 | 0 | 0 |
| 588 | 2071.181 | 0 | 0 | | 0 | | 0 | 0 | 0 |
| 591 | 2100.057 | 0 | 0 | | 0 | | 0 | 0 | 0 |
| 594 | 2630.702 | 0 | 0 | | 0 | | 0 | 0 | 0 |
| 597 | 2614.016 | 0 | 0 | | 0 | | 0 | 0 | 0 |
| 600 | 1920.657 | 0 | 0 | | 0 | | 0 | 0 | 0 |
| Sum original | light spectrum | 2155.8699 | 0 | | 12 | | 203 | 205 | Intensity after |
| | Refl. corr. | 1.35 | 400 | | 400.282317 | 400.56 | 430.033893 | 430.359135 | Scintillator: 42.4241693 |
| | Refl. loss | 0.0055 | 0.03648131 | | 0.03412294 | 0.0329 | 0.01112063 | 0.01099056 | Normalized: 0.01967845 |
| | Effective diam | 1.273 | Intensity: | | | | | | |
| | Bar Length: | 400 | 0.01967845 | | | | | | |
| | Fiber length: | 85 | 0.0171603 | | | | | | |
| | Lightguide: | 24 | 0.01646184 | | | | | | |

Fig. 8 Example of the spreadsheet layout

and bar length are given in a row along the bottom. In the intervening columns the intensity profile for each angle is given; each entry is the result of a calculation by a single exponential function based on the attenuation length for that wavelength, and scaled by the reflection loss estimate. On the rightmost part of this section the output intensity profile in the last column is given as the average of the values for each angle; since the spacing in angles is proportional to solid angle, this results in a solid angle weighted average. The sum of the entries in the output intensity profile gives the total intensity. The number of reflections as a function of angle is calculated in a row along the bottom; this taken together with an average loss per reflection gives an attenuation factor which depends on angle (and not on wavelength).

The spreadsheet contained well over 30,000 equations and occupied about 1.5 Mb on disk (half this amount after compression). On a Macintosh Quadra 800 (kindly loaned for use by the CEBAF Detector Meisters) using Microsoft Excel, performing a single iteration of the calculation required just a few seconds. Performing a calculation of the light attenuation as a function of position required about four minutes on this machine. The calculation could probably be scaled down significantly without sacrificing much accuracy; this present implementation integrated over 100 angles and 100 wavelengths for three different optical elements, which is particularly unnecessary in the case of the fiber readout where a small range of angles is involved.

## 8. Calculation Results

In Fig. 9 the results are plotted for the prediction of the final intensity distribution. Each curve is scaled to equal height to facilitate comparison of spectral shape; it is to be noted that the absolute intensity actually changes by more than an order of magnitude for the curves shown. The solid curve is the BC-412 emission spectrum. The dashed curve is the final intensity distribution for a 50 cm scintillator length. The dotted curve gives the same data for a 100 cm scintillator length, and the dot-dashed curve gives the intensity distribution for a 400 cm scintillator length. A shift to higher wavelengths is clear, and additionally the distribution acquires more structure than the original emission spectrum. The peak shifts by about 15 nm; the actual centroid of the distribution shifts by about 20 nm. Most of the shift of the centroid is due to attenuation in the scintillator since it is the longest element in the system and it is the least transparent element to wavelengths less than 420 nm (ref. Fig. 4). Since the attenuation characteristics of each optical element are similar above 425 nm, the attenuation in that region is dominated by the element for which

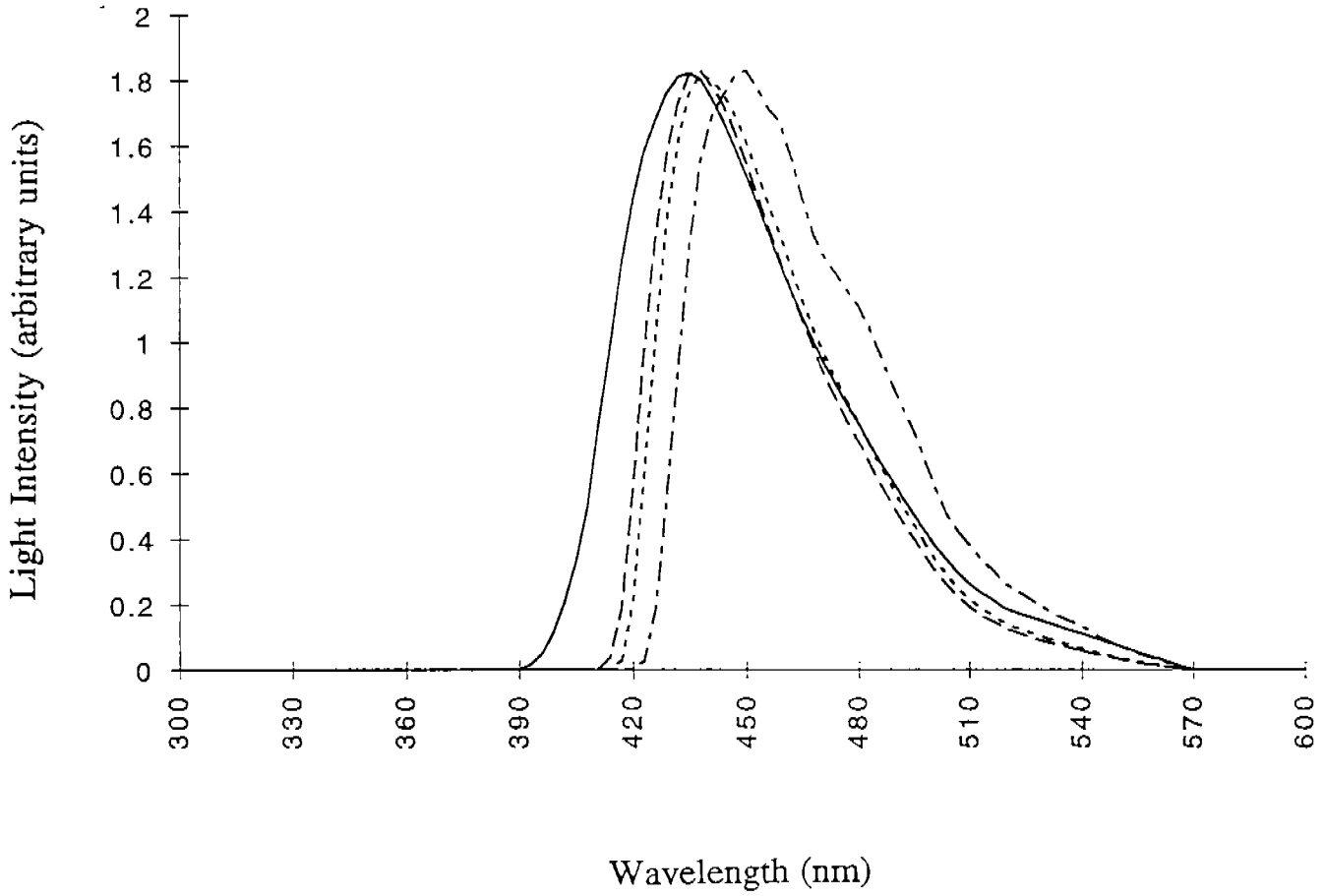


Fig. 9 Predictions of the model for spectral behavior of the fiber readout system. The first curve on the left is the emission spectrum for the scintillator. The second, third and fourth curves are the spectral output of the system for scintillator lengths of 50, 100, and 400 cm. These curves have been rescaled to the same height for comparison of shapes.

the light path is longest, which is generally the scintillator (but which could be the fiber light guide in certain cases).

In Fig. 10 is a comparison of the effect of the fiber light guide length on the final light spectrum for x = 100 cm (upper curves) and x = 400 cm (lower curves) length. The solid lines indicate the predictions for the shorter fibers, and the dashed lines are for the longer fibers. It may be seen that there is a moderate reduction in the light intensity due to the longer fibers(<10%), and that the spectral shape is modified very little.

Fig. 11 is a plot of the predicted pulse shape due to geometry alone in the fiber readout system (solid lines) and in the direct readout system coupled with coupling gel (dashed lines) for a scintillator length of 400 cm. The uppermost two curves are for unattenuated rays, while the other two curves are for rays which have been attenuated. The scintillator decay time is of the order of a few nanoseconds, and is not included here. Naively the assumption might be that the direct coupled light has a much slower response time than the fiber light, as is borne out by the upper two curves. However, it is seen in the lower two curves that the effect of the attenuation (including reflection losses) is to dramatically shorten the time span of the directly read out light, while the fiber light is not much affected. While the integrating effect of the photomultiplier tube is not explicitly considered here, in Fig. 12 these same pulses are numerically integrated to give an approximate idea of what the discriminated pulse would look like. It may be seen that it takes about twice as long for the directly read out pulses to reach 90% of full intensity as for the fiber light, but that this still only requires about 3 ns. This is similar to the decay time of BC-412 scintillator; the real pmt pulses will fold these two times together within the integration time of the pmt and base combination. If the scintillator decay time and the above time dispersions are combined in quadrature, the model predicts a 20-25% faster rise time for the fiber readout compared to the direct readout at x = 400 cm. Although the direct readout method has a longer risetime in this model, it will tend to collect more light simply because a larger area of the scintillator is viewed (thus improving photoelectron statistics) which is likely to more than compensate the difference in risetime for equal energy deposits. (In addition there will be a different deposit pattern across the pmt face which will contribute to the timing resolution in different ways in the two coupling schemes.)

Fig. 13 through Fig. 15 are a comparison of the data measured by the teachers to the model predictions for the variation of light as a function of position along the scintillator. Figs. 13, 14, and 15 each show two smooth curves; the dashed curve is the model prediction with no reflection losses, and the smooth curve is the model prediction assuming an average reflection loss of 0.55% per reflection and the parameter $\alpha = 1.35$. (It should be noted that the surface of this test scintillator had some visible damage and

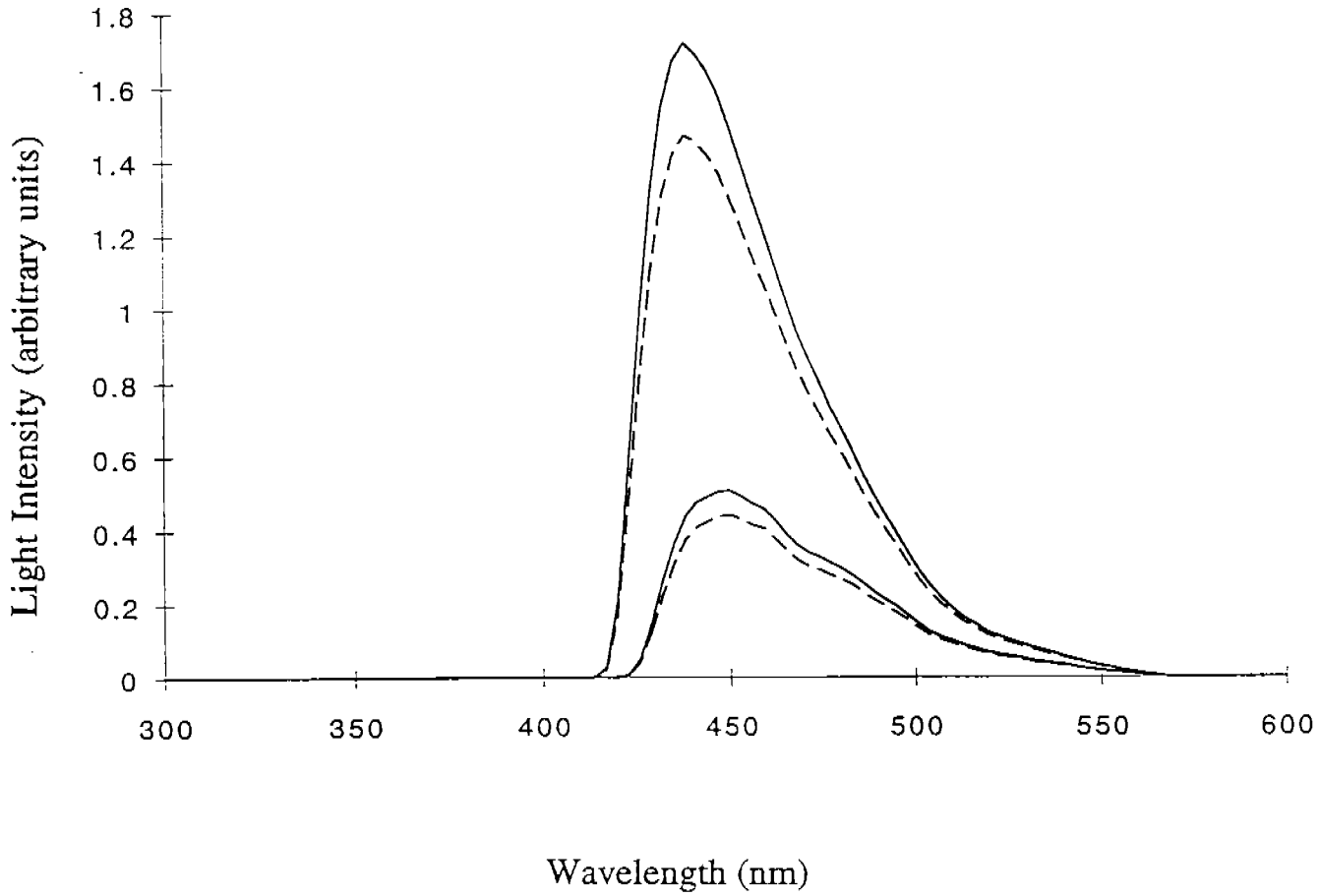


Fig. 10. Predictions of the model for the difference between the shortest (18 cm) and longest (85 cm) fiber readouts. The upper two curves are for x = 100 cm and the lower two curves are for x = 400 cm. The solid lines correspond to the short fibers and the dashed lines correspond to the long fibers.

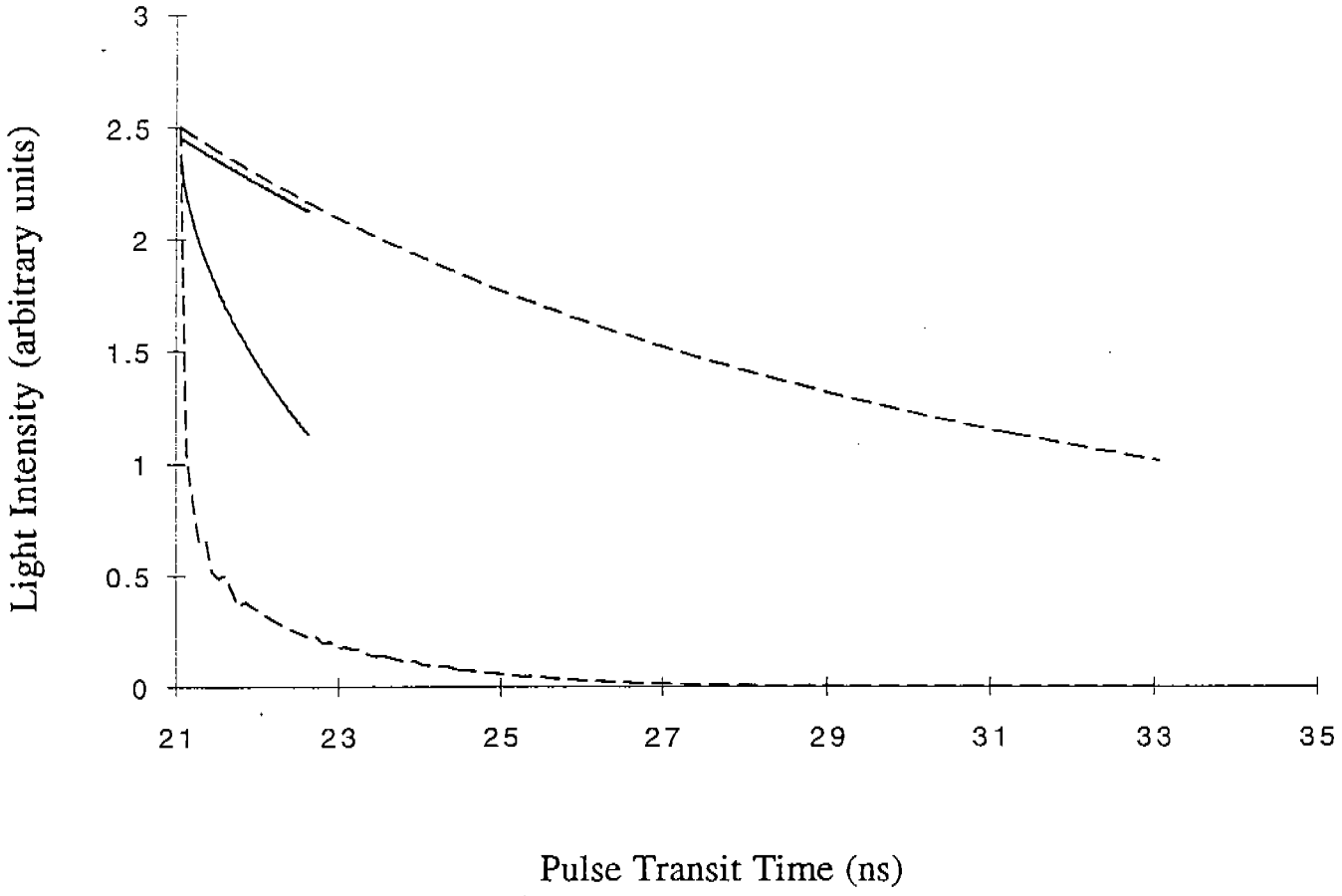


Fig. 11 Predictions of the model for the time behavior of light pulses. The upper two curves are the light pulseshape for the fiber readout system (solid curve) and the direct readout system coupled with gel (dashed curve) in the case of no attenuation. The lower two curves are the same but the light attenuation and reflection losses have been included. All curves have been rescaled for comparison.

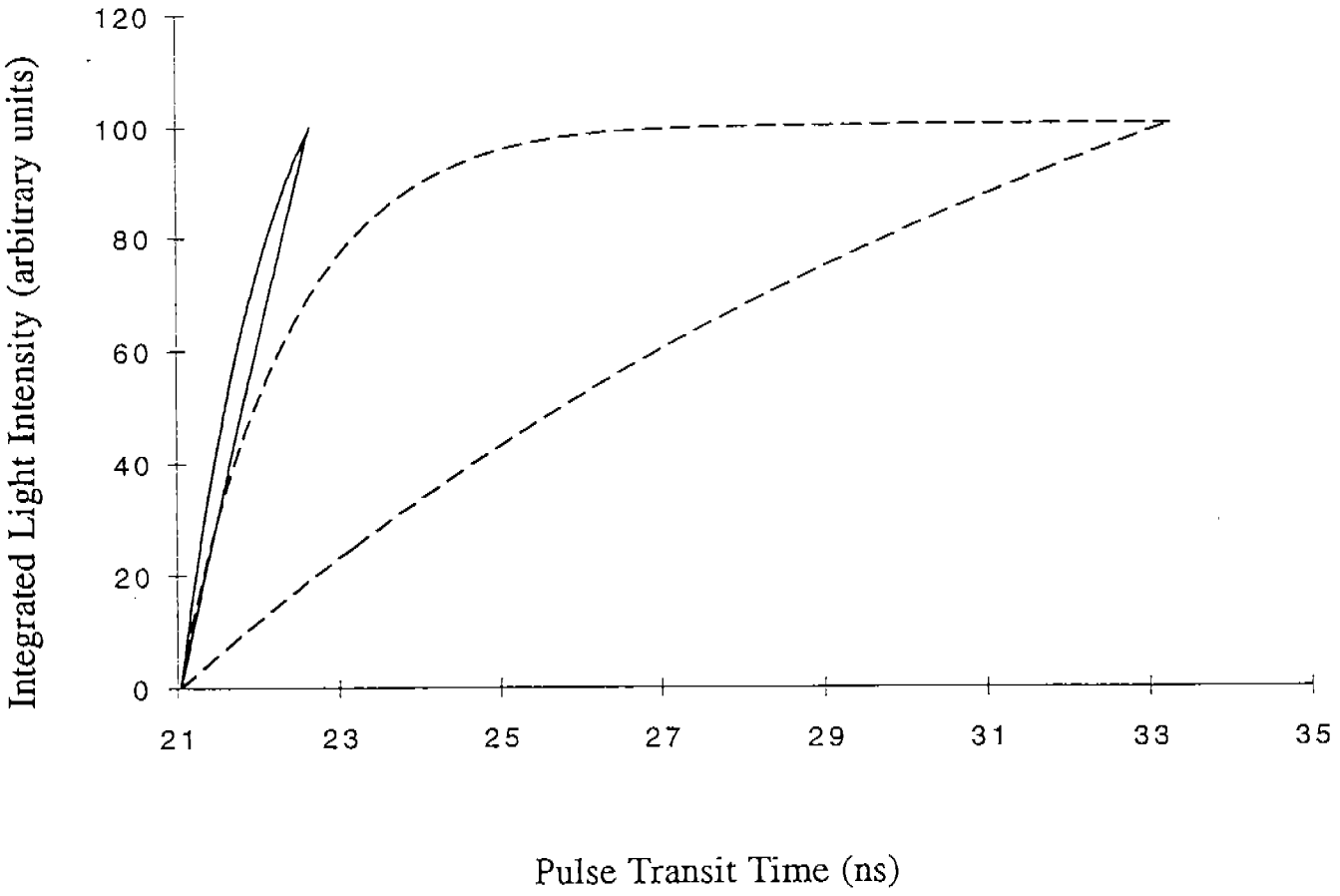


Fig. 12 Same as Fig. 11 but here the curves are integrated over time. These curves represent the expected pulse from the photo tube in the case where the scintillator decay time and the photo tube integration time are neglected. All curves have been rescaled for comparison.

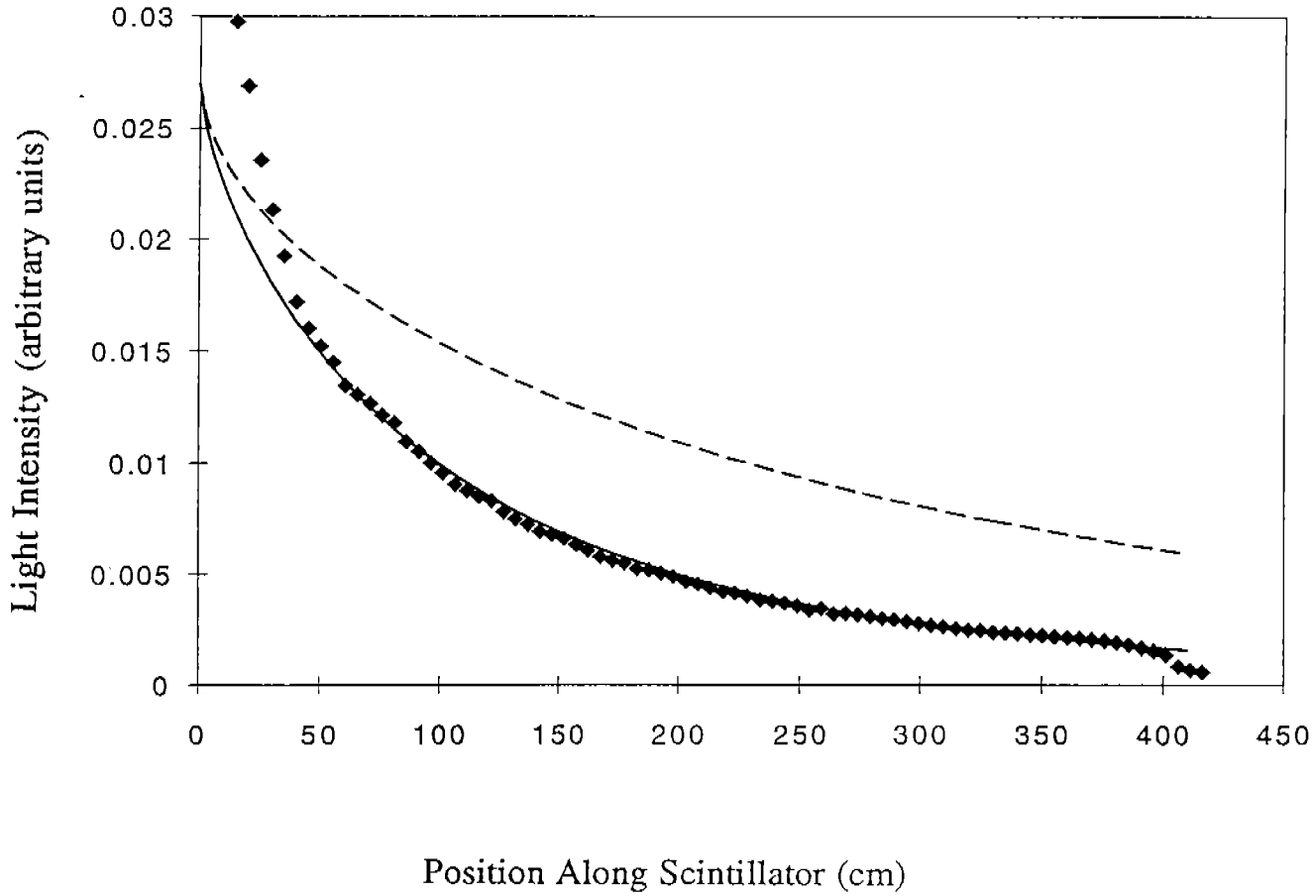


Fig. 14 Light output as a function of distance along the scintillator x for the direct readout system without coupling gel. The dotted curve is the model prediction without surface reflection losses. The solid curve is the model prediction with 0.55 % surface reflection losses and a geometrical parameter of 1.35, and the data is approximately normalized to this curve.

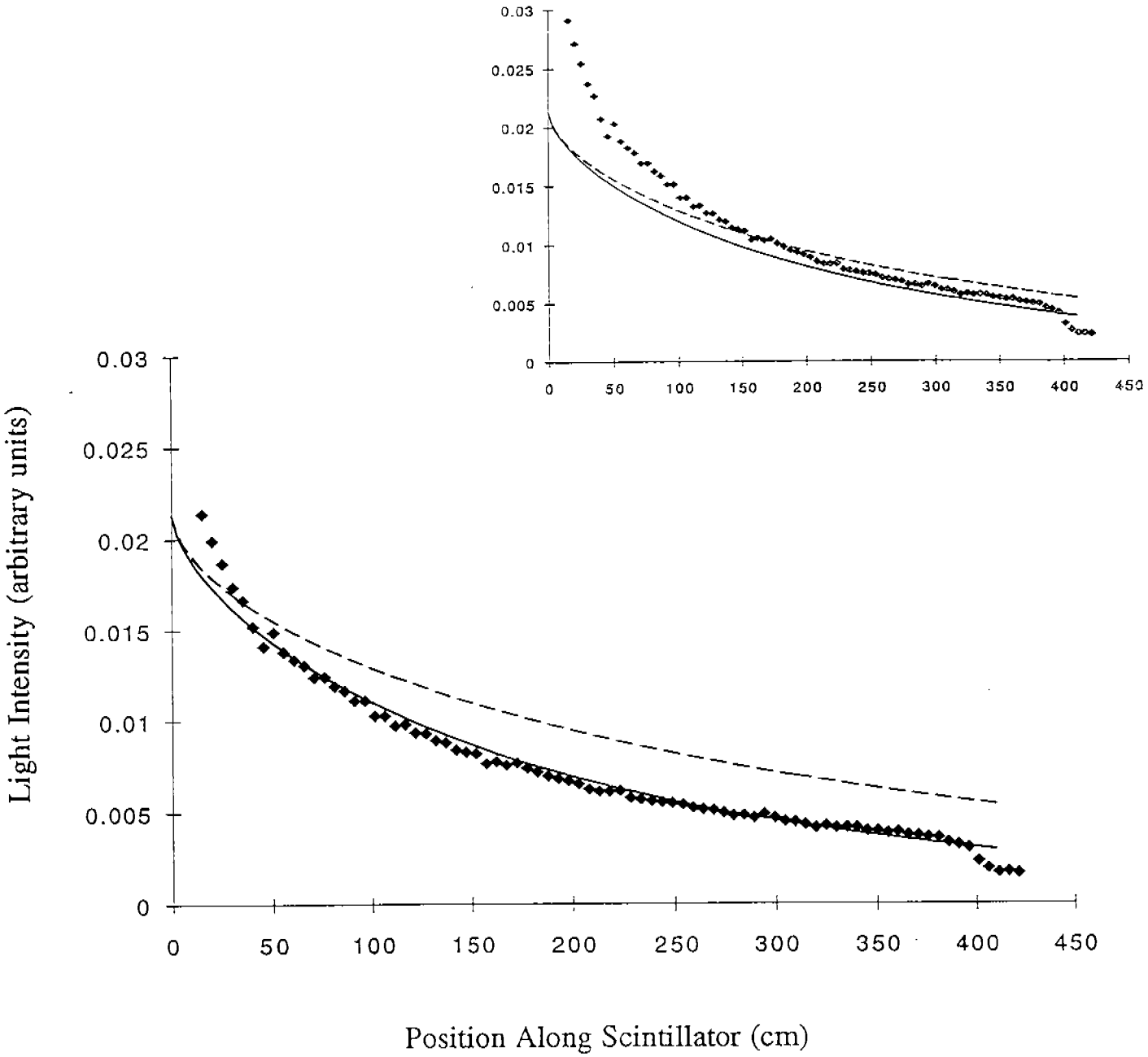


Fig. 13 Light output as a function of distance along the scintillator x for the fiber readout system. The dotted curve is the model prediction without surface reflection losses. The solid curve is the model prediction with 0.55 % surface reflection losses and a geometrical parameter of 1.35, and the data is approximately normalized to this curve. The inset plot is the same with the data normalized to the upper curve.

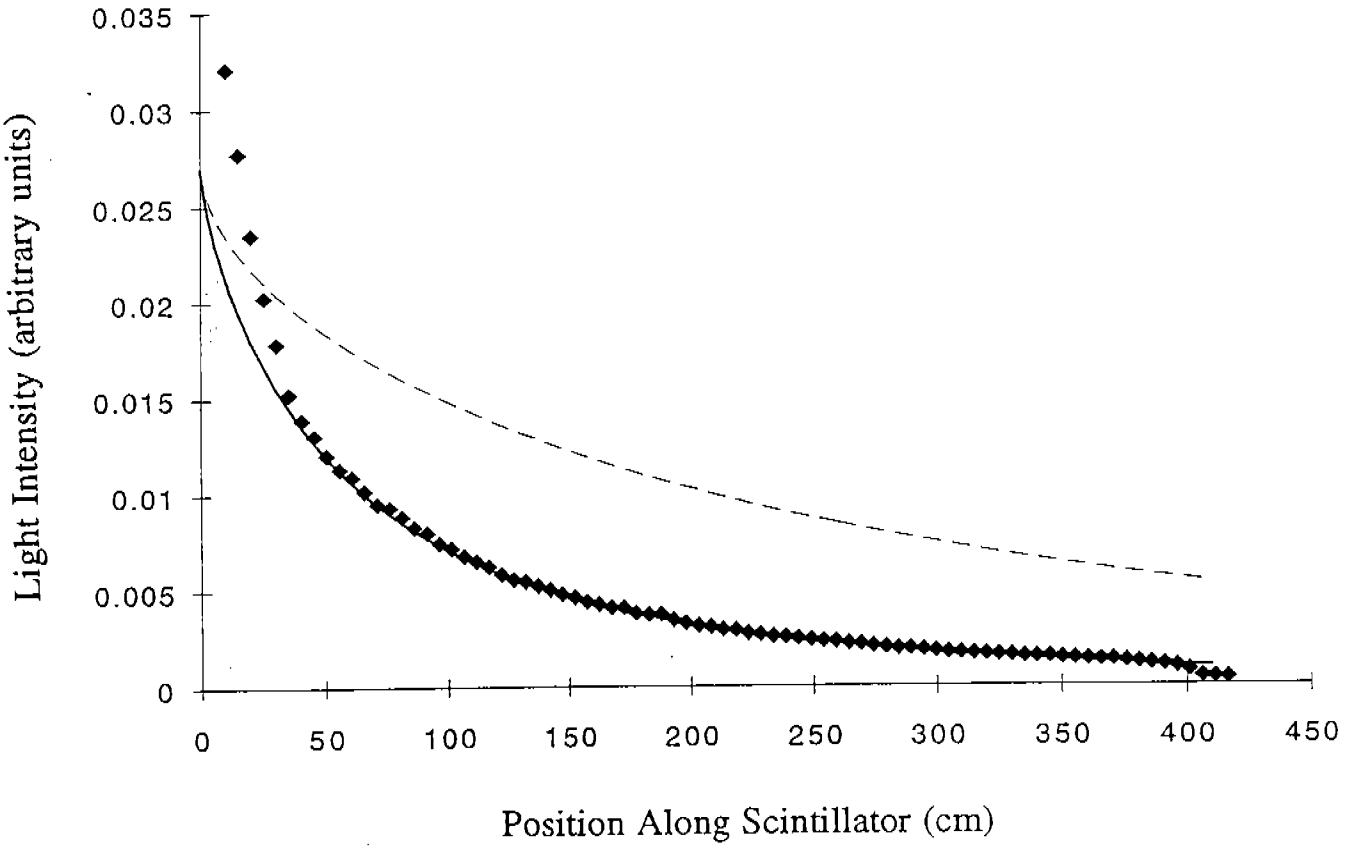


Fig. 15 Light output as a function of distance along the scintillator x for the direct readout system with coupling gel. The dotted curve is the model prediction without surface reflection losses. The solid curve is the model prediction with 0.55 % surface reflection losses and a geometrical parameter of 1.35, and the data is approximately normalized to this curve.

therefore the reflection loss parameter is likely to be worse than for an average new scintillator.) These parameters were adjusted to give the best agreement with the data. Fig. 13 shows a comparison of the model fit for the fiber data, Fig. 14 shows a comparison for the directly coupled (no gel) data, and Fig. 15 shows a comparison for the directly coupled (with gel) data. The inset plot in Fig. 13 shows the data normalized to the model prediction without any reflection losses. It may be seen that a good description of the data may not be obtained without invoking the existence of reflection losses. As may be seen, the model does a very good job of fitting all of these data with only two adjustable parameters except at short distances. This is to be expected from the model assumption that the light is emitted from the center of a cylindrical light guide; this assumption is far from true for the case of few reflections with a distributed light source. The length of the source along the x direction may be estimated from the dropoff at x=400 cm (the end of the strip) seen in Fig. 13 to be approximately 5 cm.

In the case of the directly read out data in Figs. 14 and 15 the disagreement is larger at small x. This is fully to be expected since the model does not include light beyond the critical angle which arrives at the phototube. In these measurements the phototube actually sees a significant amount of light which exits the wider surfaces of the scintillator, and also intercepts light at greater than the critical angle from the end of the scintillator at very short x. Therefore, larger deviations from this calculation are expected for the directly coupled light than the fiber-coupled light, which is seen to be the case.

It should be noted that it is remarkable that these three rather complex curves can be generated with only two parameters (plus a scale factor for each curve) from a simple formula. The dashed curves are weighted averages over three hundred exponentials in the case of the fiber data, and one hundred exponentials in the case of the direct readout data. The solid curves are substantially different in shape for the three cases, and are multiplicative corrections to the dashed curves in a power law of a complicated function. The agreement seen with the data indicates that the model contains the few essential ingredients needed to explain these data for $x > 50$ cm.

## 9. Conclusions

A simple conceptual model has been constructed for internally reflected light in an optical system. The model has been implemented in a spreadsheet calculation as a research tool and as an educational tool. There are a variety of predicted results from the model. A spectral peak shift of approximately 15 nm and a centroid shift of about 20 nm are expected for x=400 cm for the emitted light from BC412 in this system. The difference in light

intensity is predicted to be less than 10% between light passing through the shortest (18 cm) and the longest (85 cm) fibers. The risetime of pulses from the fiber system is predicted to be about 25% smaller than for the directly coupled system at x=400 cm. The shapes of the light intensity as a function of x are well predicted using a 2 parameter scaling prescription with an average light loss per reflection of 0.55% and a geometrical parameter of 1.35. These paramters simultaneously produce the best fit to the data measured for all three coupling schemes. The agreement with the data indicates that the model contains all the essential features of the systems studied for $x > 50$ cm. It is likely that improved results for $x < 50$ cm would be obtained with a Monte Carlo calculation which would more precisely model the small x behavior of the system.

## 10. References


1. R. L. Garwin, Rev. Sci. Instr. 23, 755 (1952).
2. CLAS-NOTE 92-012
3. Catalog of Bicron Corp., 12345 Kinsman Rd., Newbury OH 44065-9677.
4. Catalog of Thorn-EMI, 100 Forge Way Unit F, Rockaway N. J. 07866.